Linköping University Post Print

Wurtzite-structure $Sc_{1-x}Al_xN$ solid solution films grown by reactive magnetron sputter epitaxy: structural characterization and first-principles calculations

Carina Höglund, Jens Birch, Björn Alling, Javier Bareño, Zsolt Czigány, Per O. Å. Persson, Gunilla Wingqvist, Agne Zukauskaite and Lars Hultman

N.B.: When citing this work, cite the original article.

Wurtzite structure Sc$_{1-x}$Al$_x$N solid solution films grown by reactive magnetron sputter epitaxy: Structural characterization and first-principles calculations

Carina Höglund,[1,a)] Jens Birch,[1] Björn Alling,[2] Javier Bareño,[1] Zsolt Czigány,[3] Per O. Å. Persson,[1] Gunilla Wingqvist,[1] Agne Zukauskaite,[1] and Lars Hultman[1]

[1]*Department of Physics, Chemistry and Biology (IFM), Thin Film Physics Division, Linköping University, SE-581 83 Linköping, Sweden*
[2]*Department of Physics, Chemistry and Biology (IFM), Theory and Modeling Division, Linköping University, SE-581 83 Linköping, Sweden*
[3]*Research Institute for Technical Physics and Materials Science, Hungarian Academy of Sciences, P.O. Box 49, HU-1525 Budapest, Hungary*

AlN(0001) was alloyed with ScN with molar fractions up to ~22%, while retaining a single-crystal wurtzite (w-) structure and with lattice parameters matching calculated values. Material synthesis was realized by magnetron sputter epitaxy of thin films starting from optimal conditions for the formation of w-AlN onto lattice-matched w-AlN seed layers on Al$_2$O$_3$(0001) and MgO(111) substrates. Films with ScN contents between 23% and ~50% exhibit phase separation into nanocrystalline ScN and AlN, while ScN-rich growth conditions yield a transformation to rocksalt structure Sc$_{1-x}$Al$_x$N(111) films. The experimental results are analyzed with ion beam analysis, x-ray diffraction, and transmission electron microscopy, together with *ab initio* calculations of mixing enthalpies and lattice parameters of solid solutions in wurtzite, rocksalt, and layered hexagonal phases. © *2010 American Institute of Physics*. [doi:10.1063/1.3448235]

I. INTRODUCTION

Solid solutions between two binary compounds, so called pseudobinary alloys, have successfully been used for band gap engineering and lattice matching in group III nitrides, mainly intended for optoelectronic devices. Pseudobinary alloys formed between the group IIIA semiconducting AlN, GaN, and InN make it possible to continuously vary the band gap aiming for a large variety of applications within optoelectronics.[1] Some of these alloys have large miscibility gaps, though, making them difficult to synthesize with industrial high temperature growth techniques like chemical vapor deposition. For such applications, increasing focus is put on pseudobinary alloys consisting of a mixture of transition metal nitrides (TMNs) and group IIIA nitrides. Such alloys could combine some of the excellent properties of pure group IIIA nitrides with the high hardness and high temperature stability that TMNs are known for.

The in-plane lattice mismatch between rocksalt (c-) ScN and wurtzite (w-) GaN is less than 2%, for ScN(111)‖GaN(0001) and ScN[110]‖GaN[1$\bar{2}$10], making ScN/GaN heterostructures or Sc$_{1-x}$Ga$_x$N solid solutions potential replacements for In$_{1-x}$Ga$_x$N.[2] Calculations of formation energies indicate that the formation of wurtzite alloys (GaN ground state) becomes more favorable than cubic alloys (ScN ground state), for GaN concentrations larger than 65%.[2] The band gap is observed to increase linearly from 2.0 to 3.5 eV with decreasing ScN content from 100% to 0%, respectively, independent of crystal structure.[2,3]

ScN is a semiconducting group IIIB nitride with an indirect band gap of 0.9–1.6 eV.[4–7] It has a rocksalt structure with an experimentally measured lattice parameter of 4.50 Å,[8] a hardness of 21 GPa,[9] and a high temperature stability with a melting temperature of 2600 °C.[10] ScN has also been suggested to exist as a metastable hexagonal (h-) ScN phase.[11] The c/a ratio of this structure is smaller than that of the wurtzite structure ($c_h/a_h \approx 1.20$ versus $c_w/a_w = 1.63$). The internal parameter u, which is the relative displacement between the metal and nitrogen sublattices, also differs considerably ($u_h = 0.5$ versus $u_w = 0.375$).[11]

Semiconducting w-AlN has been extensively studied, mainly for optical, acoustic, and electronic device applications, due to its attractive physical properties like wide energy band gap (6.2 eV),[12] high hardness (>20 GPa),[13,14] high thermal conductivity (3.19 W/cm K at RT),[15] piezoelectric coefficient of $d_{33} = 5.5$ pCN^{-1},[16] and high temperature stability (melting point >2000 °C).[17] Its lattice parameters are $a = 3.11$ Å and $c = 4.98$ Å, yielding a relaxed c/a ratio of 1.6. [ICDD PDF 25-1133]

Sc–Al–N is still an unexplored material system. The only reported ternary compound is the inverse perovskite Sc$_3$AlN.[18,19] There are a few experimental papers dealing with the solid solution Sc$_{1-x}$Al$_x$N, published very recently. We have thus reported that AlN molar fractions of up to ~60% can be dissolved into c-Sc$_{1-x}$Al$_x$N(111), epitaxially deposited onto a ScN(111) seed layer.[20] Higher AlN contents result in phase separation into wurtzite structure (w-)AlN or AlN-rich w-Sc$_{1-x}$Al$_x$N, with up to four epitaxial relationships to the seed layer. Akiyama *et al.* reported on textured Sc$_{1-x}$Al$_x$N thin films, with $0.54 \leq x \leq 1$, deposited by reactive rf dual-magnetron sputtering onto Si(001) substrates. For substrate temperatures of 580 °C, the films were said to be wurtzite structured for $x \geq 0.59$, cubic for $x \leq 0.54$, and consist of a mixture of structures for $0.55 \leq x \leq 0.58$.[21] Their

a)Electronic mail: carina@ifm.liu.se.

results show also that the piezoelectric response of alleged $Sc_{1-x}Al_xN$ solid solutions improves with increasing Sc content but that it has a strong dependence on growth temperature. Lowering the substrate temperature to 400 °C yielded better crystalline quality[22] and a good crystalline quality is said to be necessary for a high piezoelectric response. For films grown at 400 °C and x=0.57, the piezoelectric coefficient d_{33} is measured to be 27.6 pCN^{-1}, which is considered to be the highest reported to date for nitride semiconductors.[22] We propose to synthesize single-crystal samples in order to enable accurate measurements of the piezoelectric coefficient in $Sc_{1-x}Al_xN$.

Here, we consider epitaxially grown solid solutions of AlN and ScN in $Sc_{1-x}Al_xN$, where Sc and Al are positioned on the metal sublattice. The magnetron sputter epitaxy (MSE) deposition technique is employed, starting from optimal conditions for growing w-AlN and performing experiments with an increasing ScN concentration until the transformation to the cubic phase like in Ref. 20 is observed. The as-deposited films are characterized using a combination of ion beam analysis, x-ray diffraction (XRD), and electron microscopy techniques. In order to gain further insight into the $Sc_{1-x}Al_xN$ system, the experimental procedure is complemented with first-principle theoretical modeling within a density functional theory framework. Solid solutions, as found in the present experiments, were considered in the modeling using a random metal sublattice configuration rather than the small sized ordered structures that have been used in previous theoretical studies on related materials.[2,23,24] The significance of this treatment for the configurational degree of freedom is described in Ref. 25. The results show that ScN molar fractions up to ~22% can dissolved into w-AlN, while retaining a single-crystal structure with lattice parameters matching calculated values.

II. EXPERIMENTAL PROCEDURES

The deposition experiments were performed in an ultrahigh-vacuum chamber at a base pressure of 1.33×10^{-6} Pa. MSE using unbalanced type II magnetrons with 50 mm diameter Sc and 75 mm diameter Al elemental targets were used to grow 50 nm thick AlN(0001) seed layers onto polished $10 \times 10 \times 0.5$ mm^3 Al_2O_3(0001) and MgO(111) substrates, followed by ~80 nm thick films of $Sc_{1-x}Al_xN$, with x ranging from 0.28 to 1. The MSE system is described in detail elsewhere.[26]

w-AlN was selected as seed layer to provide the best possible hexagonal template for basal plane growth of w-$Sc_{1-x}Al_xN$, especially for the films with high Al content. MgO(111) and Al_2O_3(0001) were used as substrate materials because they are temperature stable and provide a reasonable lattice match to the AlN seed layer, with a lattice mismatch of 4.45% and 11.97%, respectively.

Prior to deposition, the substrates were cleaned in ultrasonic baths of trichloroethylene, acetone and 2-propanol, and blown dry in dry N$_2$. This was followed by degassing in the vacuum chamber at 900 °C for 1 h before ramping down to the substrate temperature of 800 °C, controlled by a thermocouple positioned behind the substrate and calibrated by py-

rometry. The seed layer and film depositions were carried out in pure N$_2$, with a partial pressure of 0.46 Pa. The substrate potential was set to be floating.

The magnetron power for the AlN seed layers was set to 250 W. For the $Sc_{1-x}Al_xN$ layers, the Al magnetron powers were 250, 230, 180, 130, or 80 W for five different depositions, while the Sc magnetron powers were adjusted accordingly to keep a total power of 250–260 W. This yielded a deposition rate of approximately 0.7 Å/s for all compositions.

A complementary deposition series was performed in order to more exactly determine the lattice parameters of the w-$Sc_{1-x}Al_xN$ solid solution. These films were deposited under similar conditions onto Al_2O_3(0001), but without seed layers, to avoid peak overlaps in XRD.

The film compositions and impurity levels were determined by elastic recoil detection analysis (ERDA), using a 40 MeV $^{127}I^{9+}$ beam at 67.5° incidence and 45° scattering angle and evaluated with the CONTES code.[27] Rutherford backscattering spectroscopy (RBS), using a 2 MeV He+beam at 6° incidence and 172° scattering angle was used to look for possible interdiffusion between layers. The crystal structure was characterized by Cu K_α XRD using a Philips Bragg–Brentano diffractometer. A Philips X'Pert MRD diffractometer, using Cu K_α radiation, with a four-axis goniometer, and configured with 1×1 mm^2 crossed slits on the primary side and 0.27° parallel plate collimator as secondary optics, was used to determine the a and c lattice parameters from specular 0002 and nonspecular $10\bar{1}5$ reflections. Cross-sectional transmission electron microscopy (TEM) was carried out with an FEI Tecnai G2 TF 20 UT FEG microscope operated at 200 kV. The same instrument, equipped with a high-angle annular dark field (HAADF) detector was used for scanning TEM (STEM), employing a subnanometer sized electron probe to resolve the sample structure. To increase the amount of incoherently scattered electrons for a predominant mass contrast image and to decrease the coherently scattered electrons, reducing the diffraction contrast, a camera length of 100 mm was used, resulting in a minimum acceptance angle of 72 mrad.

First-principles calculations of the mixing enthalpies and lattice parameters in cubic, wurtzite, and hexagonal $Sc_{1-x}Al_xN$ solid solutions were carried out within a density functional theory framework. The projector augmented wave method as implemented in the VIENNA *AB INITIO SIMULATION PACKAGE* (Refs. 28–30) was used together with the generalized gradient approximation (GGA) (Ref. 31) for the exchange-correlation functional. The nitrogen sublattice was considered to be fully stoichiometric. The metal sublattice was modeled as a random alloy with the special quasirandom structures (SQS) model, which was first suggested by Zunger *et al.*,[32] and further developed by us.[33] The calculations of the wurtzite and hexagonal structures were done for 128 atoms SQS-supercells while the calculations for the cubic phase used the SQS reported in Ref. 33. In all calculations local lattice relaxations and optimization of the c/a ratio (for the wurtzite and hexagonal phases) was performed independently for each considered volume and composition.
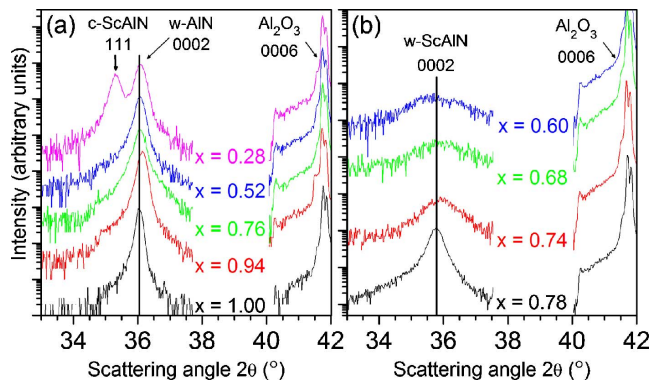
FIG. 1. (Color online) XRD data from epitaxial $Sc_{1-x}Al_xN$ films deposited on (a) $Al_2O_3(0001)$ substrates with w-AlN(0001) seed layers, with varying Al fraction, x, from 0.28 to 1 and (b) $Al_2O_3(0001)$ substrates with varying x from 0.60 to 0.78.

FIG. 2. (Color online) Lattice parameters c in (a) and a in (b) vs composition x for w-$Sc_{1-x}Al_xN$ films, showing experimental data (dots) and calculated values (squares). The lines are guide for the eye.

III. RESULTS AND DISCUSSION

Compositional analyses of the $Sc_{1-x}Al_xN$ films and AlN seed layers deposited onto MgO (111) substrates were mainly performed with ERDA. All seed layers and films are stoichiometric with respect to nitrogen to within ± 3 at. %. The Al to Sc molar ratios are 100/0, 94/6, 76/24, 52/48, and 28/72, yielding AlN molar fractions, x=1.00, 0.94, 0.76, 0.52, and 0.28, respectively. For the complementary samples, we used x=0.78, 0.74, 0.68, and 0.60. The level of impurities is low in all samples with O being the most common impurity at a maximum level of ~ 2 at. % in films with the highest Sc contents. All samples present an increased amount of O close to the surface, consistent with postdeposition surface oxidation rather than O contamination during the growth process. C and H were also present at levels close to the detection limit (~ 0.1 at. %) in all films.

RBS confirmed the compositions obtained by ERDA. This technique also yielded sharp edges for all elemental peaks of both Sc and Al (in agreement with Ref. 20), showing that there has been no interdiffusion between substrates, (seed layers) and films despite the relatively high deposition temperature.

Figure 1 shows the XRD data from $Sc_{1-x}Al_xN$-films. In Fig. 1(a), x ranges from 0.28 to 1.00 on $Al_2O_3(0001)$ substrates with AlN(0001) seed layers. For all film compositions, the Al_2O_3 0006 substrate and AlN 0002 seed layer peaks can clearly be seen. For x=0.94, the AlN 0002 peak slightly shifts toward higher angles but no additional peaks originating from the films are visible for $0.52 \leq x \leq 1.00$. Due to the severe peak overlap between seed layer and film, no further conclusions about the solubility of ScN into w-AlN can be drawn from these samples. In order to avoid the $Sc_{1-x}Al_xN$-AlN peak overlap, we consider the complementary series of $Sc_{1-x}Al_xN$ films deposited onto Al_2O_3 substrates without the AlN seed layer. XRD data from four of these samples are shown in Fig. 1(b), for comparison. The position of the $Sc_{1-x}Al_xN$ peak is seen to be almost stationary. According to φ-scans, the film is a single-crystal for x =0.78. For $x \leq 0.74$, the crystalline quality starts to decrease, even though the film peak never vanishes for concentrations
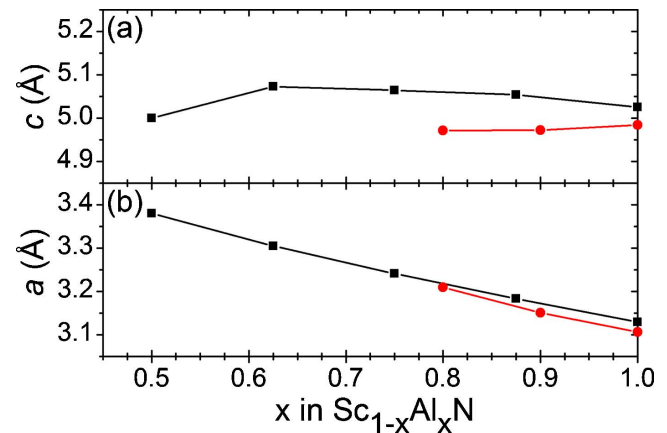
$x \geq 0.60$. We conclude that the films are almost completely phase separated into ScN and AlN with a nanocrystalline structure at such high contents of Sc.

For the $Sc_{0.72}Al_{0.28}N$ film, an additional peak appears at $2\theta = 35.3°$ in the XRD scan in Fig. 1(a). The peak position is similar to that for c-$Sc_{0.71}Al_{0.29}N(111)$ in Ref. 20 and this corresponds to a cubic lattice parameter of 4.40 Å. Pole figures confirm that the film is cubic with a $\langle 111 \rangle$ growth direction. Here, we note that even though the deposition parameters differ in the two studies, depositions of $Sc_{1-x}Al_xN$ films with $x \leq 0.29$ yield cubic structures, which follow the lattice parameter trends in Fig. 6 of Ref. 20.

Similar for all measurements is that the c-parameter of w-$Sc_{1-x}Al_xN$ is close to constant for all Sc concentrations. In order to understand this behavior the results of lattice parameters calculated with our theoretical scheme are presented in Fig. 2 (black squares), together with lattice parameters that were measured with XRD (red dots). As can be seen in Fig. 2(a), the calculated c-parameter is indeed not changing much upon Sc alloying to x as low as 0.50, with a maximum deviation from the values of pure w-AlN of only 0.3%. A slight overestimation of experimental lattice spacings in the calculations is normal when using a GGA exchange-correlation functional. As mentioned above, the overlapping peaks of w-AlN and w-$Sc_{1-x}Al_xN$ make it impossible to see from which phase that the residual intensity in the XRD scans from films with high Sc contents stems.

The calculations also reveal an almost linear decrease in wurtzite a-parameter with increasing Al content, as seen in Fig. 2(b). The difference between x=0.5 and 1 is almost 8%. XRD measurements of a-parameters in films with good enough crystalline quality to allow for the measurements, are added into the graph and they follow the calculated trend well.

TEM images were recorded from three samples (x =0.94, 0.78, and 0.28) along the $[2\bar{1}\bar{1}0]$ and $[10\bar{1}0]$ zone axes of the Al_2O_3 substrate. The overview image in Fig. 3(a) shows the Al_2O_3 substrate, the AlN seed layer, and the $Sc_{0.06}Al_{0.94}N$ film along the $(2\bar{1}\bar{1}0)$ zone axis. Both film and seed layer consist of epitaxial columnar domains with boundaries defined by threading defects. The interface be-
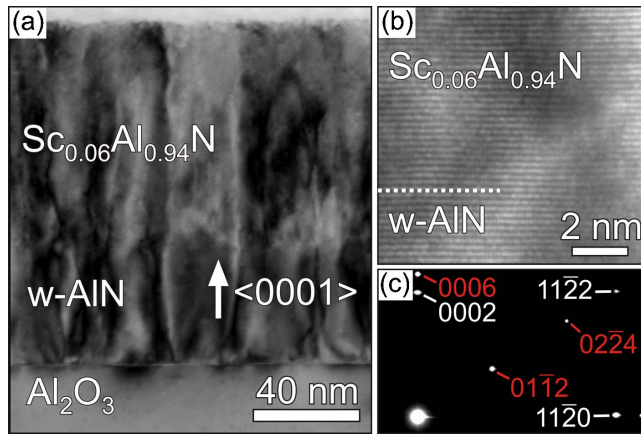
FIG. 3. (Color online) TEM micrographs from a w-$Sc_{0.06}Al_{0.94}N$ film deposited onto a Al_2O_3(0001) substrate with a w-AlN(0001) seed layer showing (a) an overview image along the $[2\bar{1}\bar{1}0]$ zone axis with the growth direction indicated and (b) the interface between film and seed layer in high resolution. In the corresponding SAED pattern (c) along the $[2\bar{1}\bar{1}0]$ zone axis of Al_2O_3, the Al_2O_3 reflections are indexed in red (gray) and overlapping w-AlN and w-$Sc_{0.06}Al_{0.94}N$ reflections are indexed in white.

tween substrate and seed layer is smooth, there is no clear interface between seed layer and film due to the relatively low Sc content in the film, and the film surface is smooth. The high resolution TEM image in Fig. 3(b) shows that the interface between the seed layer and film has weak contrast. The crystalline quality is high, however, the defect density is slightly higher in the film compared to the seed layer.

The selected area electron diffraction (SAED) pattern from the sample, obtained along the $[2\bar{1}\bar{1}0]$ zone axis of the Al_2O_3 substrate in Fig. 3(c), contains indexed reflections from Al_2O_3, AlN, and $Sc_{0.06}Al_{0.94}N$. A comparison with a SAED pattern (not shown) from only Al_2O_3 and AlN shows that both seed layer and film have the same wurtzite structure. The $Sc_{0.06}Al_{0.94}N$ reflections are not broadened, showing that there are no variations in lattice parameter, which supports the findings from XRD that the film is a disordered single-crystal solid solution with almost the same lattice parameters as AlN.

Figure 4(a) shows an overview image of the Al_2O_3 substrate, the AlN seed layer, and the $Sc_{0.24}Al_{0.76}N$ film along the $[2\bar{1}\bar{1}0]$ zone axis of Al_2O_3. While the substrate and seed layer look the same as in the previous sample, the crystal quality of the film has deteriorated with increasing Sc content and the image is dominated by spatially limited strain contrast. The high resolution TEM image in Fig. 4(b) shows a qualitative difference between seed layer and film, with significantly more defects in the film compared to the single-crystal seed layer.

A narrow columnar pattern appears in the $Sc_{0.24}Al_{0.76}N$ film when studied by HAADF-STEM, see Fig. 4(c). This pattern is not present in the w-AlN seed layer, which exhibits a homogenous mass contrast. This is a strong indication for that a phase separation has occurred, between what is perceived to be ScN and AlN-rich domains in the $Sc_{0.24}Al_{0.76}N$ film. The domain size is of the order of a few nanometers, which explains why this structure does not give any intensity in XRD measurements. It further agrees with the localized strain contrast seen in the TEM image.
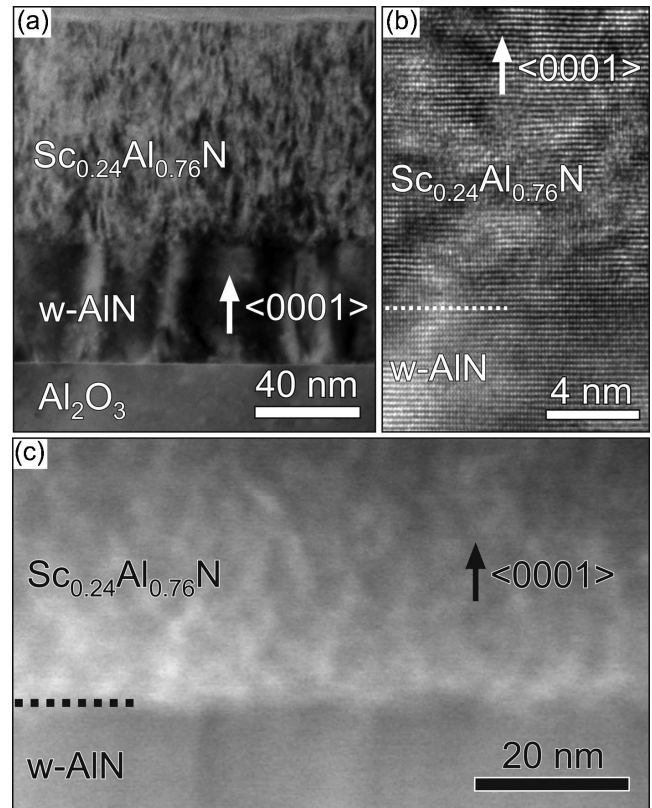

FIG. 4. $Sc_{0.24}Al_{0.76}N$ film deposited onto a Al_2O_3(0001) substrate with a w-AlN(0001) seed layer showing (a) an overview TEM micrographs along the $[2\bar{1}\bar{1}0]$ zone axis with the growth direction indicated, (b) the interface between film and seed layer in high resolution, and (c) a STEM image of the interface between film and seed layer.

Figure 5 shows the results from a TEM study of the c-$Sc_{0.72}Al_{0.28}N$ film. The overview image in Fig. 5(a), taken along the $[2\bar{1}\bar{1}0]$ zone axis of Al_2O_3, shows that on top of the substrate and seed layer, the film appears to have an epitaxial columnar structure, high defect density, and a rough surface. The corresponding high resolution TEM image in Fig. 5(b) shows that there is a higher density of defects in the film than in the seed layer.

The SAED pattern from the c-$Sc_{0.72}Al_{0.28}N$ film looks similar to the w-$Sc_{0.06}Al_{0.94}N$ film, with an in-plane broadening of the film reflections [see Fig. 3(c)]. The film, however, has a cubic crystal structure and grows along the $\langle 111 \rangle$-direction, as was confirmed with pole figures (not shown). Therefore, along the $[10\bar{1}0]$ zone axis of Al_2O_3 in Fig. 5(d) the film and seed layer diffraction patterns appear different. The film pattern in orange (light gray) corresponds to a cubic crystal structure along the $[10\bar{1}]$ zone axis.

In order to gain further understanding of $Sc_{1-x}Al_xN$ solid solutions, which were shown above to be disordered, a systematic theoretical first-principles study was performed of the mixing enthalpies of the different relevant crystal structures: the cubic B1, wurtzite B4, as well as the suggested metastable hexagonal ScN.[11] In Ref. 20, the zinc-blende B3, structure was found to be considerably higher in energy as compared to cubic and wurtzite phases for $Sc_{0.5}Al_{0.5}N$ and is thus excluded from this analysis. The cubic solid solution has been considered over the whole concentration range $0 \leq x$

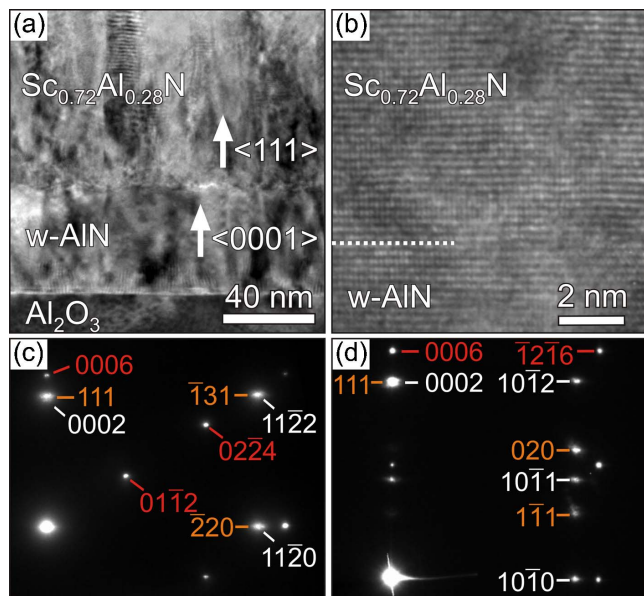FIG. 5. (Color online) TEM micrographs from a c-$Sc_{0.72}Al_{0.28}N$ film deposited onto Al_2O_3(0001) substrate with a w-AlN(0001) seed layer showing (a) an overview image along the Al_2O_3 $[2\bar{1}\bar{1}0]$ zone axis with the growth direction indicated and (b) the interface between film and seed layer in high resolution. (c) and (d) show corresponding SAED patterns along the $[2\bar{1}\bar{1}0]$ and $[10\bar{1}0]$ zone axes of Al_2O_3, respectively, where Al_2O_3 reflections are indexed in red (gray), w-AlN reflections are indexed in white and c-$Sc_{0.72}Al_{0.28}N$ reflections are indexed in orange (light gray).

≤ 1, the wurtzite in the range 0.375 ≤ x ≤ 1 and the hexagonal structure over the range 0 ≤ x ≤ 0.5. The resulting enthalpies with respect to w-AlN and c-ScN are plotted in Fig. 6. All structures are found to have high positive mixing enthalpies indicating that they can only be created experimentally as metastable phases with an inherent driving force for clustering and phase separation. This result is in line with the absence of such phases in the equilibrium bulk phase diagram in Ref. 19. Even at high temperatures, up to the melting point of AlN of 2000 °C,[17] only dilute solutions are likely to be stabilized by configurational entropy. However, it is well
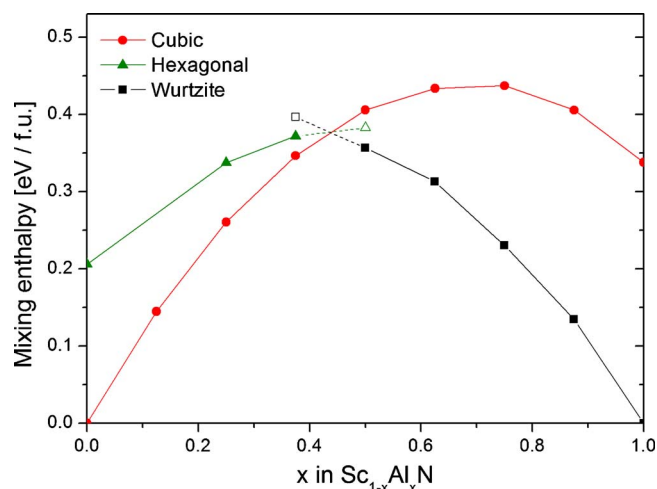

FIG. 6. (Color online) Calculated mixing enthalpies for cubic, wurtzite, and hexagonal crystal structures in $Sc_{1-x}Al_xN$, with 0 ≤ x ≤ 1. The points highlighted with open symbols might not correspond to local energy minima but at least saddle points. The lines are guides for the eye.
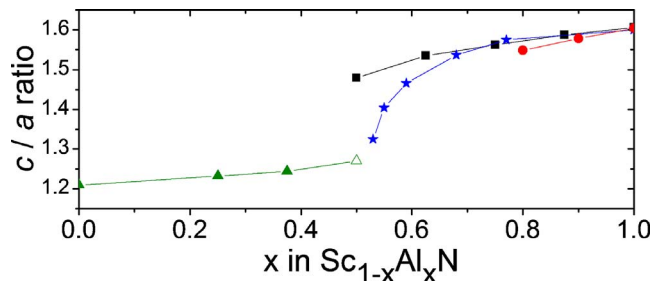

FIG. 7. (Color online) c/a lattice parameter ratios plotted over composition x in $Sc_{1-x}Al_xN$ for experimental data from present work (red dots), experimental data replotted from Ref. 21 (blue stars), calculated values for wurtzite structure (black squares), and calculated values for hexagonal structure (green triangles), with the open symbol corresponding to a ratio derived from what might be an energy saddle point.

established that off-equilibrium thin-film growth, such as reactive MSE used in this work, can inhibit phase separation during growth due to ion-bombardment induced mixing and kinetically limited deposition conditions.[34] Instead metastable, high entropy, solid solutions are formed and the relative energetics between the different structures of such solutions is a factor deciding the outcome.[35] According to the results in Fig. 6, the rocksalt structure is energetically most favorable for concentrations x ≤ 0.45, while higher AlN concentrations promote the wurtzite structure. The hexagonal structure is not the most favorable structure for any composition but close to $Sc_{0.5}Al_{0.5}N$ all three structures are almost degenerate in energy. Due to the small energy difference between hexagonal and wurtzite phases at x=0.375 and 0.50 we are within the calculation uncertainties not able to conclude whether the higher energy phases correspond to stable local energy minima or just saddle points, with respect to change mainly in the c/a ratio. The points in question are highlighted with open symbols in Fig. 6 and are investigated elsewhere.[36] These results indicate that $Sc_{1-x}Al_xN$ solid solutions should tend to form in the cubic structure for x ≤ 0.45 and in the wurtzite structure for x ≥ 0.45, while there is no region implicated for a stable hexagonal phase. This is in line with the present experimental work and the results in Ref. 20, even though the results in Ref. 20 indicate that as high as ~60 at. % AlN can be forced into solid solution with ScN while keeping the cubic structure. The comparison to experiment underlines the importance of the structure of the seed layers that help to extend the composition regime of phase formation in preference of its own structure.

In Fig. 7 the results of calculated c/a lattice spacing ratios of h- and w-$Sc_{1-x}Al_xN$ versus composition are plotted together with experimental data from Fig. 2 and replotted experimental data from Ref. 21. Even though the c/a ratio of the hexagonal structure increases from 1.21 for x=0.00 to 1.24 for x=0.50, and for the wurtzite structure decreases from 1.61 for x=1.00 to 1.48 for x=0.50, there is still a considerable difference in lattice spacing for the compositions (x=0.5) where both the wurtzite and hexagonal phases have been considered in Fig. 6. In the present series of experiments we see no indication of h-$Sc_{1-x}Al_xN$. It should, though, be noted that the growth of films in Ref. 21 results in a clear decrease in the c/a ratio upon increase in ScN con-
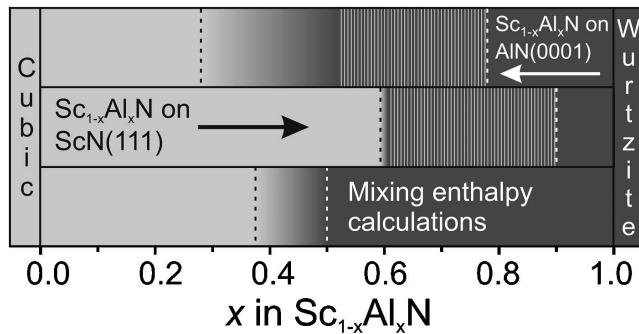
FIG. 8. Schematic phase-composition diagram for $Sc_{1-x}Al_xN$ solid solutions, for $0 \le x \le 1$. The upper row shows $Sc_{1-x}Al_xN$ films deposited onto AlN(0001) seed layers starting from optimal conditions for w-AlN, the middle row illustrates $Sc_{1-x}Al_xN$ films deposited onto ScN(111) seed layers starting from ScN from Ref. 20, and the lower row shows expected crystal structures according to mixing enthalpy calculations. The gradient areas between cubic and wurtzite structures correspond to an unexplored range of compositions in the different cases and the striped areas correspond to a two phase regime.

tent, in comparison to our calculated values. According to calculations performed by Tasnádi *et al.* in Ref. 36, the increased piezoelectric response observed in Ref. 21 is explained by a competition between the wurtzite and hexagonal phases of $Sc_{1-x}Al_xN$. For $Sc_{0.50}Al_{0.50}N$, the wurtzite structure's global energy minimum is connected with a shallow region originating from residues of h-ScN. The reported continuous change in the c/a ratio in Ref. 21 for $0.5 \le x \le 0.65$ in relation to our calculated equilibrium values indicates that the films in the same reference are subject to lattice strain, giving a particularly large impact in films with high Sc contents due to lattice softening, as discussed in Ref. 36.

This study combined with the results from Refs. 20 and 21 also illustrates the difficulties in controlling the deposition of polytype solid solutions. The schematic drawing in Fig. 8 shows the resulting phase for different compositions. The data from this study are drawn in the upper row, indicating that $x \ge 0.78$ yields films with wurtzite structure and $x \le 0.28$ yields cubic films, providing deposition conditions optimal for w-AlN. Exactly at which composition between $0.28 \le x \le 0.52$ the transitions to a single phase cubic structure occurs has not yet been pinpointed. For the series of c-$Sc_{1-x}Al_xN$ in Ref. 20, it was shown that the transition from a cubic structure to a mixture of cubic and wurtzite structures takes place at $x \approx 0.6$, as is shown in the middle row in Fig. 8. The results from mixing enthalpy calculations in the lower row in Fig. 8, however, indicate that the transition should take place at $x \approx 0.45$. This means that there is a compositional range from $\sim 0.45 \le x \le 0.6$ where wurtzite, cubic, and hexagonal phases are possible. The experimental and theoretical efforts in this work as well as the recent results in Refs. 20–22 and 36 concerning the Sc–Al–N system have shown that the relative energies of the solution phases, although important, do not fully determine the preferred structure and growth orientations, and that deposition parameters (e.g., the choice of seed layer and growth temperature) exert a critical influence on the final film structure.

IV. CONCLUSIONS

Thin films of $Sc_{1-x}Al_xN$, with x varied from 0.28 to 1.00, were deposited by reactive MSE onto MgO(111) and Al_2O_3(0001) substrates kept at 800 °C from elemental Al and Sc targets, under conditions optimal for growth of w-AlN(0001). ScN molar fractions of $\sim$22% have been dissolved into AlN, forming a disordered single-crystal solid solution of w-$Sc_{1-x}Al_xN$(0001). The measured lattice parameters agree with calculated values, meaning that the a-parameter increases almost linearly from 3.11 to 3.21 for x varied between 1.0 and 0.80, while no significant change in the c-parameter is observed in the same compositional interval. ScN contents between 23% and $\sim$50% yield a nanocrystalline mixture of ScN and AlN phases and even higher ScN contents result in solid solutions of our recently reported c-$Sc_{1-x}Al_xN$. *Ab initio* calculations of mixing enthalpies and lattice parameters of bulk solid solutions with wurtzite, cubic, and hexagonal structures predict the transition from cubic to wurtzite structures at $x \sim 0.45$, which deviates from the experimentally reported transition at x=0.60. The present work thus contributes to the understanding of the Sc–Al–N system as well as the general differences between relaxed bulk thermodynamics and epitaxial thin-film growth of multinary nitrides.

[1]T. Seppänen, Ph.D. dissertation, Linköping Studies in Science and Technology, 2006.
[2]M. G. Moreno-Armenta, L. Mancera, and N. Takeuchi, Phys. Status Solidi B **238**, 127 (2003).
[3]M. E. Little and M. E. Kordesch, Appl. Phys. Lett. **78**, 2891 (2001).
[4]W. R. L. Lambrecht, Phys. Rev. B **62**, 13538 (2000).
[5]D. Gall, M. Städele, K. Järrendahl, I. Petrov, P. Desjardins, R. T. Haasch, T.-Y. Lee, and J. E. Greene, Phys. Rev. B **63**, 125119 (2001).
[6]C. Stampfl, W. Mannstadt, R. Asahi, and A. J. Freeman, Phys. Rev. B **63**, 155106 (2001).
[7]H. A. Al-Brithen, A. R. Smith, and D. Gall, Phys. Rev. B **70**, 045303 (2004).
[8]W. Lengauer, J. Solid State Chem. **76**, 412 (1988).
[9]D. Gall, I. Petrov, N. Hellgren, L. Hultman, J.-E. Sundgren, and J. E. Greene, J. Appl. Phys. **84**, 6034 (1998).
[10]K. A. Gschneider, Jr., G. A. Melson, D. A. Melson, D. H. Youngblood, and H. H. Schock, in *Scandium: Its Occurrence*, edited by C. T. Horovitz (Academic, London, 1975), Vol. 165, cited in Ref. 32.
[11]N. Farrer and L. Bellaiche, Phys. Rev. B **66**, 201203(R) (2002).
[12]S. Strite and H. Morkoc, J. Vac. Sci. Technol. B **10**, 1237 (1992).
[13]P. Limsuwan, N. Udomkan, S. Meejoo, and P. Winotai, Int. J. Mod. Phys. B **19**, 2073 (2005).
[14]A. Kumar, H. L. Chan, J. J. Weimer, and L. Sanderson, Thin Solid Films **308–309**, 406 (1997).
[15]G. A. Slack, R. A. Tanzilli, R. O. Pohl, and J. W. Vandersande, J. Phys. Chem. Solids **48**, 641 (1987).
[16]R. C. Turner, R. E. Fuierer, R. E. Newnham, and T. R. Shrout, Appl.

Acoust. **41**, 299 (1994).

[17]C. F. Cline and J. S. Kahn, J. Electrochem. Soc. **110**, 773 (1963).

[18]J. C. Schuster and J. Bauer, J. Less-Common Met. **109**, 345 (1985).

[19]C. Höglund, J. Birch, M. Beckers, B. Alling, Zs. Czigány, A. Mücklich, and L. Hultman, Eur. J. Inorg. Chem. **2008**, 1193 (2008).

[20]C. Höglund, J. Bareno, J. Birch, B. Alling, Zs. Czigány, and L. Hultman, J. Appl. Phys. **105**, 113517 (2009).

[21]M. Akiyama, T. Kamohara, K. Kano, A. Teshigahara, Y. Takeuchi, and N. Kawahara, Adv. Mater. (Weinheim, Ger.) **21**, 593 (2009).

[22]M. Akiyama, K. Kano, and A. Teshigahara, Appl. Phys. Lett. **95**, 162107 (2009).

[23]A. Alsaad and A. Ahmad, Eur. Phys. J. B **54**, 151 (2006).

[24]S. Zerroug, F. Ali Sahraoui, and N. Bourissa, J. Appl. Phys. **103**, 063510 (2008).

[25]B. Alling, A. Karimi, and I. Abrikosov, Surf. Coat. Technol. **203**, 883 (2008).

[26]J. Birch, S. Tungasmita, and V. Darakchieva, *Vacuum Science and Technology: Nitrides as Seen by Technology* (Research Signpost, Trivandrum, 2002), pp. 421–456.

[27]M. S. Janson, CONTES Conversion of Time-Energy Spectra—a program for ERDA data analysis, Internal report, Uppsala University, 2004.

[28]P. E. Blöchl, Phys. Rev. B **50**, 17953 (1994).

[29]G. Kresse and J. Hafner, Phys. Rev. B **48**, 13115 (1993).

[30]G. Kresse and J. Furthmüller, Comput. Mater. Sci. **6**, 15 (1996).

[31]J. Perdew, K. Burke, and M. Ernzerhof, Phys. Rev. Lett. **77**, 3865 (1996).

[32]A. Zunger, S. H. Wei, L. G. Ferreira, and J. E. Bernard, Phys. Rev. Lett. **65**, 353 (1990).

[33]B. Alling, A. V. Ruban, A. Karimi, O. E. Peil, S. I. Simak, L. Hultman, and I. A. Abrikosov, Phys. Rev. B **75**, 045123 (2007).

[34]P. H. Mayrhofer, C. Mitterer, L. Hultman, and H. Clemens, Prog. Mater. Sci. **51**, 1032 (2006).

[35]H. Holleck, Surf. Coat. Technol. **36**, 151 (1988).

[36]F. Tasnádi, B. Alling, C. Höglund, G. Wingqvist, J. Birch, L. Hultman, and I. A. Abrikosov, Phys. Rev. Lett. **104**, 137601 (2010).